

Surface-Initiated Polymerization of 5-(Perfluoro-*n*-alkyl)norbornenes from Gold Substrates

Christopher J. Faulkner, Remington E. Fischer, and G. Kane Jennings*

Department of Chemical and Biomolecular Engineering, Vanderbilt University, Nashville, Tennessee 37235

Received October 9, 2009; Revised Manuscript Received November 25, 2009

ABSTRACT: We report the surface-initiated ring-opening metathesis polymerization (SI-ROMP) of 5-(perfluoro-*n*-alkyl)norbornenes (NBF*n*) to grow partially fluorinated polymer films of tunable thicknesses ranging from tens of nanometers to micrometers on gold substrates. The perfluoroalkyl chains range in length (*n*) from 4 to 10 carbons, representing 67–83% of the molecular weight of the repeat unit. The growth rate of the film depends on the perfluoroalkyl chain length, with longer chains enabling faster surface-initiated growth and greater ultimate thicknesses. These films exhibit hydrophobic and oleophobic surface properties and provide effective barriers to the diffusion of aqueous ions. The critical surface tensions of the films exhibit a minimum for a fluorocarbon chain of 8 (pNBF8) and range from 9 to 19 mN/m. The morphologies of the pNBF*n* films consist of densely packed 20–30 nm clusters that differ in the concentration of fluorocarbon chains in the outer few nanometers of the film.

Introduction

Because of their low critical surface energy,¹ dielectric constant,² and chemical inertness,³ fluorinated polymers are used for a wide range of applications including protective coatings, biomaterials,⁴ membranes,⁵ and microelectronics.⁶ Recently, more attention has been given to partially perfluorinated polymers because of concerns over the safety and processability of perfluorinated polymers. Partially fluorinated polymers are advantageous over perfluorinated polymers as the desired interfacial and surface properties of the fluorocarbon moiety can be achieved and, in many cases, surpassed, using safer, simpler, and less expensive methods.

Generally, fluorinated polymers are deposited onto surfaces via spin-coating,⁷ dip-coating,⁸ solution-casting,⁹ or chemical adsorption.¹⁰ In the case of spin-coating and solution-casting, uniform polymer film coatings are possible on planar surfaces. However, these methods do not provide a direct attachment of the polymer to the surface, nor can they be applied to nonplanar geometries. Chemical adsorption yields nonconformal, low-density polymer films due to steric and diffusional constraints of untethered polymer segments.¹⁰

Surface-initiated polymerizations (SIP) enable controlled growth of polymer chains that are directly attached to a surface and are capable of producing conformal thin films on surfaces of many geometries.¹¹ Generally, surface-initiated polymer films obtain their fluorocarbon functionality through postprocessing methods. Our group¹² has modified poly(hydroxyethyl methacrylate) (PHEMA) films with perfluorinated acid chlorides to obtain fluorocarbon functionality throughout the film and achieve critical surface energies as low as 9 mN/m. Bruening, Baker, and co-workers have used postfluorination of PHEMA to prepare membranes capable of high CO₂ permeability and CO₂/CH₄ selectivity.⁵

The ability to achieve partially perfluorinated polymer films directly via surface-initiated polymerization would eliminate the need for postprocessing methods mentioned in the examples

above. However, few partially fluorinated polymers have been grown directly from a surface using surface-initiated polymerizations. A notable example includes the work of Ruhe and co-workers, who polymerized a fluorinated acrylate using controlled radical polymerization methods.¹³ They were able to achieve dense films; however, the polymerization required 4 and 27 h to achieve films ~20 and ~70 nm thick, respectively. In general, controlled radical polymerization methods require hours to yield coherent polymer films less than 100 nm thick.^{14,15} An exception is water-accelerated atom transfer polymerization (ATRP), which exhibits much faster kinetics enabling the growth of thicker polymer films, > 100 nm.^{16–18} However, monomers must be water-soluble, thus precluding the use of most fluorinated monomers in water-accelerated ATRP.

In this article, we describe the preparation of partially fluorinated polymer films using surface-initiated ring-opening metathesis polymerizations (SI-ROMP). SI-ROMP is attractive for its mild reaction conditions and rapid kinetics to enable films with thicknesses of several nanometers up to a few micrometers.^{2,19} The predominate ROMP monomers studied in surface-initiated cases have been norbornene and its functional derivatives,^{2,20–23} due to their high reactivity of norbornene in ROMP and the ease of synthesizing functionalized monomers. Here, we have synthesized 5-(perfluoro-*n*-alkyl)norbornenes (NBF*n*) with fluorocarbon chain lengths (*n*) of 4, 6, 8, and 10 and polymerized them from surfaces using Grubbs second-generation catalyst (Figure 1). Our approach combines the advantages of SI-ROMP with the technological importance of partially fluorinated films to grow tunable films under ambient conditions.²⁴ We show that these films grow rapidly, are far more stable than polynorbornene films, and yield critical surface tensions that are dependent on the fluorocarbon chain length.

Experimental Methods

Materials. Gold shot (99.99%) was obtained from J&J Materials, and silicon (100) wafers were purchased from Montico Silicon. Chromium-coated tungsten rods were obtained from R.D. Mathis. Deionized water (16.7 MΩ) was purified using a Modu-Pure filtration system, and 200 proof ethanol was

*To whom correspondence should be addressed; e-mail kane.g.jennings@vanderbilt.edu, Tel 615-322-2707, Fax 615-343-7951.

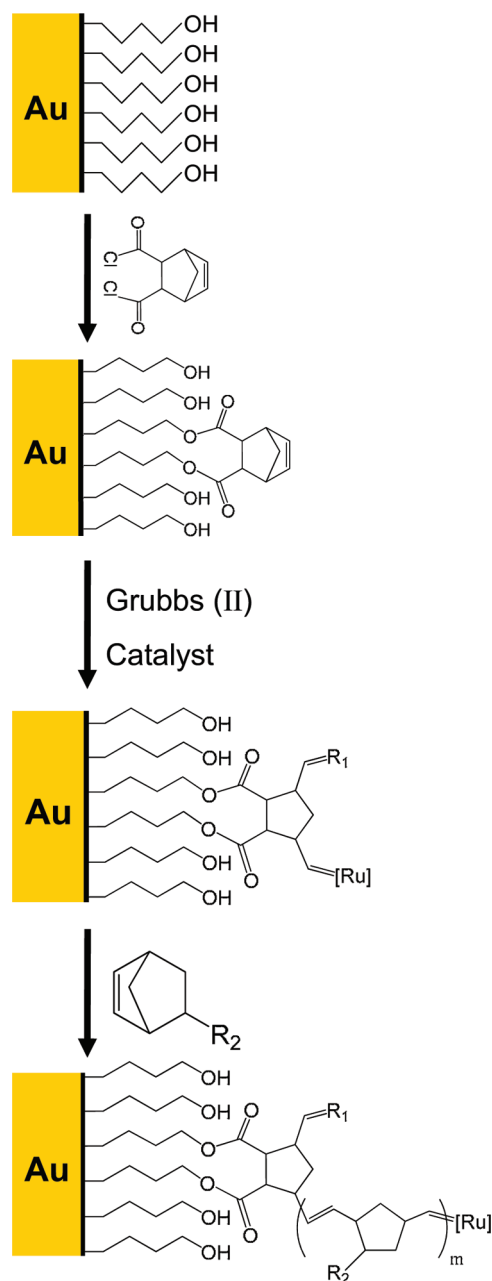
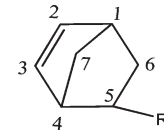


Figure 1. Schematic of SI-ROMP of 5-(perfluoro-*n*-alkyl)norbornenes on a gold substrate. A gold surface is modified with mercaptobutanol and further treated with *trans*-5-norbornene-2,3-dicarbonyl chloride for 30 min. The initiator is activated by Grubbs second-generation catalyst, denoted as [Ru], and exposed to the NBF*n* monomer solution ($R_2 = -C_4F_9$, $-C_6F_{13}$, $-C_8F_{17}$, or $-C_{10}F_{21}$). R_1 represents CHPh.

used as received from Aaper. The following chemicals were obtained from Sigma-Aldrich and used as received: Grubbs catalyst—first generation (benzylidene-bis(tricyclohexylphosphine)dichlororuthenium), Grubbs catalyst—second generation (1,3-bis(2,4,6-trimethylphenyl)-2-(imidazolidinylidene)(dichlorophenyl)methylene), 1*H*,1*H*,2*H*-perfluoro-1-hexene (99%), 1*H*,1*H*,2*H*-perfluoro-1-octene (99%), 1*H*,1*H*,2*H*-perfluoro-1-decene (99%), hydroquinone, 1,4-mercaptobutanol, 1,2,4-trichlorobenzene, and 2,2,2-trifluoroethanol. Dicyclopentadiene (95%), *trans*-3,6-endomethylene-1,2,3,6-tetrahydrophthaloyl chloride (97%), and *n*-hexadecane (99%) were purchased from Acros Organics. 1*H*,1*H*,2*H*-Perfluoro-1-dodecene (97%) was purchased from Matrix Scientific. *n*-Decane (99%), *n*-dodecane (99%), and *n*-tetradecane (99%) were purchased from Alfa Aesar, and *n*-hexane (95%), methylene chloride

Table 1. Summary of ^{13}C NMR Spectra for all pNBF*n* Monomers



monomer	isomer	^{13}C δ (ppm)						
		C ₁	C ₂	C ₃	C ₄	C ₅	C ₆	C ₇
NBF4	exo	41.1	138.2	136.2	42.3	40.6	26.7	46.3
	endo	41.9	137.2	131.7	43.5	40.8	27.4	49.6
NBF6	exo	41.1	138.1	136.2	42.3	40.6	26.7	46.2
	endo	41.9	137.1	131.6	43.5	40.7	27.4	49.5
NBF8	exo	41.2	138.2	136.3	42.4	40.6	26.7	46.3
	endo	42.0	137.2	131.7	43.6	40.7	27.5	49.6
NBF10	exo	41.1	138.1	136.2	42.3	40.6	26.7	46.2
	endo	41.9	137.1	131.6	43.5	40.9	27.4	49.5

(DCM), chloroform, and 1,2-dichloroethane were purchased from Fisher.

Synthesis of NBF*n*. Four monomers were synthesized utilizing a Diels–Alder reaction described by Perez et al.:²⁵ 5-(perfluorobutyl)norbornene (NBF4), 5-(perfluorohexyl)norbornene (NBF6), 5-(perfluorooctyl)norbornene (NBF8), and 5-(perfluorodecyl)norbornene (NBF10), with ~47%, 48%, 47%, and 50% yield, respectively. Briefly, a Parr Instruments high-pressure reaction vessel was charged with 1:1 molar ratios of the 1*H*,1*H*,2*H*-perfluoro-1-alkene and dicyclopentadiene and 0.03 mole fraction of hydroquinone, as a quenching agent. The reaction was held at 170 °C for 72 h. Monomers were purified by vacuum distillation. A DRX-400 Bruker NMR spectrometer equipped with a 9.4 T Oxford magnet was used to confirm the chemical structure and composition of the synthesized 5-(perfluoro-*n*-alkyl)norbornenes (NBF*n*). The reactions yielded ~3:1 ratio of endo- to exo-isomers of the NBF*n* as determined by ^{13}C NMR. The NMR spectra were collected using deuterated chloroform as solvent and are consistent with those reported by Perez et al. NBF4: ^1H NMR (CDCl_3): δ 6.2, 6.0 (2H), 3.2 (1H), 3.0 (1H), 2.8 (1H), 2.0 (1H), 1.5 (1H), and 1.2–1.4 (2H). ^{19}F NMR (CDCl_3): δ -81.0 (s); -112.8 (m); -123.8 to -121.4 (m); -127.1 to -125.1 (m). NBF6: ^1H NMR (CDCl_3): δ 6.2, 6.0 (2H), 3.2 (1H), 3.0 (1H), 2.8 (1H), 2.0 (1H), 1.5 (1H), and 1.2–1.4 (2H). ^{19}F NMR (CDCl_3): δ -80.9 (s); -112.6 (m); -123.8 to -121.3 (m); -127.1 to -125.3 (m). NBF8: ^1H NMR (CDCl_3): δ 6.2, 6.0 (2H), 3.2 (1H), 3.0 (1H), 2.8 (1H), 2.0 (1H), 1.5 (1H), and 1.2–1.4 (2H). ^{19}F NMR (CDCl_3): δ -81.0 (s); -112.6 (m); -123.8 to -121.4 (m); -127.2 to -125.4 (m). NBF10: ^1H NMR (CDCl_3): δ 6.2, 6.0 (2H), 3.2 (1H), 3.0 (1H), 2.8 (1H), 2.0 (1H), 1.5 (1H), and 1.2–1.4 (2H). ^{19}F NMR (CDCl_3): δ -80.9 (s); -112.6 (m); -123.9 to -121.4 (m); -127.2 to -125.5 (m). Table 1 summarizes the ^{13}C NMR spectra for all monomers.

Preparation of Gold Substrates. Gold substrates were prepared by evaporating chromium (100 Å) and gold (1250 Å) in sequence onto silicon (100) wafers at rates of 1–2 Å s⁻¹ in a diffusion-pumped chamber with a base pressure of 4×10^{-6} Torr. After removal from the evaporation chamber, the wafers were typically cut into 1.4 cm \times 4 cm pieces.

Polymerization. Gold substrates were placed in a 1.0 mM ethanolic solution of 4-mercapto-1-butanol for at least 1 h to yield a hydroxyl-terminated self-assembled monolayer (SAM). The films were rinsed in ethanol and dried in a stream of nitrogen. Exposure of the SAM to a 5 mM solution of *trans*-3,6-endomethylene-1,2,3,6-tetrahydrophthaloyl chloride in dichloromethane for 30 min yields the acylation product of a surface-tethered norbornenyl group.²⁶ The samples were rinsed with DCM, ethanol, and dried in a stream of N₂. The norbornenyl-decorated substrates were exposed to a 5 mM solution of

Grubbs II catalyst in dichloromethane for 10 min. The monolayers were rinsed with dichloromethane and immediately placed in a monomer solution containing 0.1 M NBF₄, 0.05 M NBF₆, 0.05 M NBF₈, and 0.05 M NBF₁₀ in dichloromethane for 1 min to grow pNBF_{*n*} films that were ~50 nm thick. pNBF_{*n*} films were also prepared in 0.5 M monomer solutions for 5 min to investigate the effect of fluorocarbon chain length on film growth. To determine the effects of monomer concentration on polymerization, pNBF₈ films were prepared with monomer solutions ranging from 0.005 to 1.0 M for 5 min. To obtain pNBH₄ films, Grubbs II-modified surfaces were exposed to 0.47 M NBH₄ solution for 10 min. All films were sequentially rinsed with fresh solvent, ethanol, and water and dried in a stream of nitrogen.

Characterization Methods. Reflectance absorption infrared spectroscopy (RAIRS) was performed using a Varian Excalibur FTS-3100 infrared spectrometer. The p-polarized light was incident at 80° from the surface normal. The instrument was run in single reflection mode and equipped with a universal sampling accessory. A liquid-nitrogen-cooled, narrow-band MCT detector was used to detect reflected light. Spectral resolution was 2 cm⁻¹ after triangular apodization. Each spectrum was accumulated over 400 scans using a deuterated octadecanethiol-*d*₃₇ self-assembled monolayer on gold as the background.

Ellipsometric thicknesses were determined from a J.A. Woollam M-2000DI variable angle spectroscopic ellipsometer using a two-parameter Cauchy model. Thicknesses were fit to data taken at 75° from the surface normal over wavelengths from 400 to 700 nm, using a refractive index of 1.38. Optical constants of the underlying gold used in the preparation of each sample were taken prior to polymer film deposition and used as a baseline for thickness measurements. Reported thickness values and errors represent the averages and standard deviations, respectively, from at least three different films. pNBF_{*n*} film thicknesses greater than 100 nm were determined using a Veeco Dektak 150 surface profiler because the Cauchy model does not adequately describe the data for thick pNBF_{*n*} films as the films become opaque.

A Rame-Hart contact angle goniometer with a microliter syringe was used to measure advancing and receding contact angles on static drops of water and hexadecane on the polymer surfaces. Critical surface energies of the pNBF_{*n*} films were estimated from a Zisman plot using a series of even-numbered *n*-alkanes from hexane to tetradecane as contacting liquids. The needle tip of the syringe remained inside the liquid drop while measurements were taken on both sides of ~5 μL drops. Reported values and ranges represent the average and standard deviation of values obtained from at least five independent sample preparations.

Film coverage and surface morphology were investigated using atomic force microscopy (AFM) with a JEOL 5200 scanning probe microscope (SPM). Height contrast images (20 μm × 20 μm) were collected in tapping mode using a silicon nitride tip. Scanning electron micrographs were collected using a Raith eLINE electron beam lithography tool in image mode using an accelerating voltage of 10.0 kV and a working distance of 10 mm.

Electrochemical impedance spectroscopy (EIS) was performed with a Gamry Instruments CMS300 impedance system interfaced to a personal computer. A flat-cell (EG&G Instruments) was used to expose only 1 cm² of each sample to an aqueous solution containing electrolyte and redox probes while preventing sample edges from being exposed. The electrochemical cell consisted of an aqueous solution of 1 mM K₃Fe(CN)₆, 1 mM K₄Fe(CN)₆ · 3H₂O, and 0.1 M Na₂SO₄ with a Ag/AgCl/saturated KCl reference electrode, a gold substrate counter electrode, and a gold substrate containing the film to be studied as the working electrode. All data were collected in the range from 10⁻¹ to 10⁴ Hz using 10 points per decade and were fit with an appropriate equivalent circuit model (vide infra) to determine

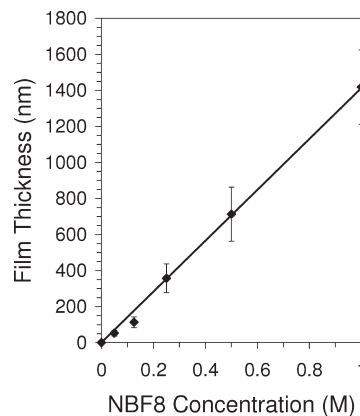


Figure 2. Effect of NBF₈ monomer concentration on pNBF₈ film thickness after exposure to the monomer in DCM for 5 min.

Table 2. Impedance Properties and Thicknesses of pNB and pNBF_{*n*} Films Grown from 1 M Monomer Solutions for 5 min

film	thickness (nm)	log(<i>R</i> _f (Ω cm ²))	<i>C</i> _f (nF/cm ²)
initiator		1.3	19 000
pNB	49	4.3	250
pNBF ₄	52	6.2	63.2
pNBF ₆	612	6.4	4.6
pNBF ₈	713	7.4	2.8
pNBF ₁₀	1565	7.5	1.6

resistance and capacitance values. Reported values and ranges for resistance and capacitance represent the average and standard deviation of values obtained from at least three independent sample preparations.

Results and Discussion

Kinetics and Concentration Effects. Films of pNBF_{*n*} were grown from gold surfaces by utilizing SI-ROMP as depicted in Figure 1. A HOC₄S/Au SAM was treated with *trans*-3,6-endomethylene-1,2,3,6-tetrahydrophthaloyl chloride, a norbornene with pendant acid chlorides in the 5- and 6-positions, to produce an ester-linked norbornene group on the surface. The resulting surface was made catalytically active for ROMP by exposure to Grubbs second-generation catalyst. Subsequent exposure to NBF_{*n*} (*n* = 4, 6, 8, and 10) in dichloromethane (DCM) resulted in the growth of partially fluorinated polymer films from the surface in times ranging from 1 to 15 min. Polymerizations that exceeded 15 min did not result in thicker films (Figure S1), as coupling and backbiting compete with metathesis and can actually result in decreased film thicknesses as observed by us¹⁸ and others.^{19,27} The rapid growth of micrometer-scale pNBF_{*n*} films by SI-ROMP contrasts the slower growth of ultrathin partially fluorinated films by ATRP.¹³ Figure 2 displays the dependence of pNBF₈ film growth on monomer concentration upon exposure to the monomer for 5 min. The linear dependence of pNBF₈ thickness with monomer concentration suggests the ability to tune film thickness from ~50 nm to a few micrometers by changing the concentration of monomer in solution. The ability to achieve film thicknesses in excess of 1 μm in as little as 5 min is attributed to the rapid turnover and activity of the surface-bound Grubbs II catalyst. All monomers showed similar trends (not shown) with increased film thicknesses at higher monomer concentrations.

Effect of Fluorocarbon Chain Length. The effect of fluorocarbon chain length (*n*) on film thickness upon exposure of Grubbs II-modified surfaces to 0.5 M NBF_{*n*} in DCM for 5 min is shown in Table 2. Whereas pNBF₄ and pNB (*n* = 0) yield similar thicknesses of ~50 nm, increasing *n* beyond

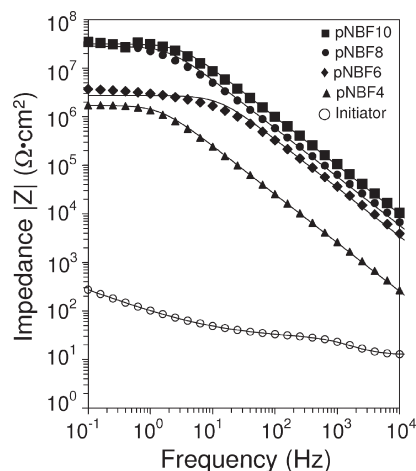


Figure 3. Electrochemical impedance spectra obtained in 1 mM $\text{K}_3\text{Fe}(\text{CN})_6$ and 1 mM $\text{K}_4\text{Fe}(\text{CN})_6$ in 0.1 M $\text{Na}_2\text{SO}_4(\text{aq})$ for the indicated films on gold prepared by exposure of Grubbs II-modified surfaces to 0.5 M NBF_n for 5 min. Solid curves represent fits of the data using appropriate equivalent circuit models.

4 results in an order-of-magnitude increase in film thickness. The large thicknesses achieved in 5 min for pNBF_n , where $n = 6, 8$, and 10 , illustrate the rapid kinetics of SI-ROMP in comparison to other surface-initiated strategies. The trend of increasing thickness with longer fluorocarbon substituents is in stark contrast to the growth of nonfluorinated pNBH_n that we observed previously.¹⁹ SI-ROMP of NBH_n yielded thinner films with more defects for increasing hydrocarbon chain length, such that polymerization of NBH_{10} generated only sparse islands of polymer.¹⁹ We attribute the dramatic increase in film growth for NBF_n monomers with $n > 4$ to the greater strain of longer chains on the norbornenyl ring to assist metathesis²⁵ as well as the structure of the predominate endo monomers in solution. Perez et al.²⁵ reported a structural conformation of endo NBF_n monomers in solution such that they adopt a folded structure in which the fluorocarbon side chain folds back toward the olefin in the norbornenyl ring. The folded structure of the monomer units obstructs access to the olefin and interferes with the metathesis polymerization. They also noted a significant reduction in the fraction of monomer that adopted the folded conformation for $n > 6$, as longer fluorocarbon chains are known to be stiff and would lack the flexibility to fold back to the olefin site. Thus, long flexible hydrocarbon chains on the norbornenyl ring would be expected to interfere with metathesis to a greater extent than would a much stiffer fluorocarbon chain of similar length.

The greater thicknesses for $n > 4$ translated into more protective coatings in an aqueous environment. We used electrochemical impedance spectroscopy to investigate the barrier properties of pNBF_n films in the presence of $\text{K}_3\text{Fe}(\text{CN})_6$ and $\text{K}_4\text{Fe}(\text{CN})_6$ in 0.1 M $\text{Na}_2\text{SO}_4(\text{aq})$. Representative Bode plots for pNBF_4 , pNBF_6 , pNBF_8 , and pNBF_{10} films that were prepared by exposure to a 0.5 M monomer solution in DCM for 5 min are shown in Figure 3. All films exhibit much higher impedance than that of the initiator SAM, and in general, the impedance at all frequencies scales with the thicknesses of these polymer films from Table 2. The thicker films provide a more complete barrier with fewer defects to minimize the penetration of the redox probes. The impedance spectra of the polymer films are best fit with a Randle's equivalent circuit²⁸ modified with a Warburg impedance term to account for a resistance to mass transfer.¹² Table 2 shows film thicknesses along with the resistances (R_f) of the

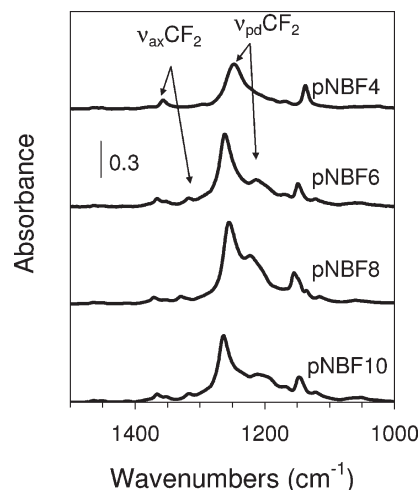


Figure 4. Reflectance absorption infrared spectra of pNBF_n films. $-\text{CF}_2$ groups primarily exhibit two modes of stretching: $\nu_{\text{ax}}(\text{CF}_2)$ from 1300 to 1400 cm^{-1} and $\nu_{\text{pd}}(\text{CF}_2)$ from 1100 to 1300 cm^{-1} .

films against penetration by redox probes and capacitance (C_f) values. The film resistances ($R_f \sim 10^{6-7} \Omega \cdot \text{cm}^2$) and capacitances ($\sim 2\text{--}63 \text{ nF}$) of pNBF_n are comparable to those of other highly blocking fluorinated polymer films.¹² Consistent with the trends of film thickness, we observed an increase in the polymer film resistance and decrease in the film capacitance with increasing perfluorinated chain length, with a dramatic decrease in capacitance for $n > 4$. When pNBF_n films of similar thickness ($\sim 50 \text{ nm}$) were characterized by EIS, the results (not shown) indicated no effect of chain length.

Film Structure. We used RAIRS to determine the composition and structure of the pNBF_n films. Figure 4 displays the fluorocarbon region of RAIR spectra for the pNBF_n films where $n = 4, 6, 8$, and 10 . The CF_2 stretching modes absorb strongly from 1100 to 1400 cm^{-1} . Because of the helical structure of fluoroalkyl chains, two types of CF_2 stretching peaks are expected in the IR: those lying along the helical axis ($\nu_{\text{ax}}(\text{CF}_2)$, 1300–1400 cm^{-1}) and those perpendicular to the helical axis ($\nu_{\text{pd}}(\text{CF}_2)$, 1100–1300 cm^{-1}).^{30–32} The ratio of $\nu_{\text{pd}}(\text{CF}_2)$ to $\nu_{\text{ax}}(\text{CF}_2)$ absorbance for the film, relative to the same ratio for isotropic orientation of drop-cast pNBF_n films, provides information on the orientation of the fluorocarbon side chains in the polymer film relative to the surface normal. RAIRS utilizes inherent surface selection²⁹ such that the intensity for a given mode in the IR spectrum is proportional to the square of the component of its dynamic dipole moment oriented along the surface normal. Figure S2 (Supporting Information) displays the RAIR spectrum for a drop-cast film of pNBF_{10} where the absorbance of $\nu_{\text{pd}}(\text{CF}_2)$ to $\nu_{\text{ax}}(\text{CF}_2)$ is nearly equal. We observe a high ratio of $\nu_{\text{pd}}(\text{CF}_2)$ to $\nu_{\text{ax}}(\text{CF}_2)$ absorbance (> 4) in the surface-initiated pNBF_n films, as shown in Figure 4, indicating the fluorinated side chains of the polymer are generally oriented more along the parallel to the gold substrate. This parallel orientation of the fluorocarbon groups is similar to that in semifluorinated polyisoprene films reported by Genzer et al.³⁰ and that reported by us for the acylation of PHEMA films with perfluorinated acid chlorides.¹²

Film Stability. pNB ($n = 0$) films have been reported as oxidatively unstable due to the unprotected olefin functionality located along the polymer backbone. Seehof and co-workers demonstrated that fluorocarbon substituents increase oxidative stability such that fluorinated polynorbornenes showed no degradation over time, whereas

unmodified pNB started to degrade within 24 h.³¹ They attribute oxidative stability to the electron-withdrawing nature of the fluorocarbon moieties, which stabilize the polymer. Elimination of chain unsaturation by sulfonation of the olefins to achieve a hydroxysulfonate product also results in more stable pNB polymer films, but sulfonation increases the solubility of any chains that were already oxidatively cleaved and may result in their removal from the film upon rinsing.²⁶ Thus, the sulfonation process itself can be used as a measure of the stability of the polymer film. Previously, we observed 40%

Table 3. Wetting Properties and Critical Surface Tensions of pNBF n Films

film	advancing contact angle (deg)		γ_C (mN/m)
	water	hexadecane	
pNBF4	110 \pm 2	61 \pm 1	19 \pm 2
pNBF6	116 \pm 5	67 \pm 1	13 \pm 1
pNBF8	123 \pm 3	78 \pm 1	9 \pm 1
pNBF10	120 \pm 3	73 \pm 2	11 \pm 1

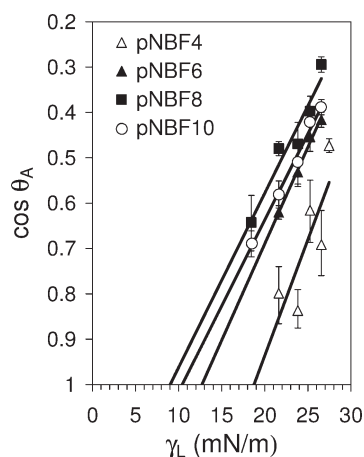


Figure 5. Zisman plot of advancing contact angles of hexane ($\gamma = 18.4$ mN/m), octane ($\gamma = 21.6$ mN/m), decane ($\gamma = 23.8$ mN/m), dodecane ($\gamma = 25.2$ mN/m), and tetradecane ($\gamma = 26.6$) on pNBF n films that were exposed to air for at least 12 h prior to measurement. The lines represent least-squares fits to the data and are extrapolated to $\cos \theta = 1.0$ to determine the critical surface energy (γ_C).

film loss of pNB films upon 1 min exposure to acetyl sulfate.²⁶ However, negligible film loss was observed during the sulfonation of pNBF4 over a 24 h exposure to acetyl sulfate.³² The improved stability imparted by the fluorocarbon side chains is likely the result of diluting olefin functionality within the film to inhibit reactions such as coupling and backbiting that are known to cleave chain fragments.^{33–35} For $n \geq 4$, the fluorocarbon chain consists of $\geq 77\%$ of the mass of the monomer repeat unit.

Surface Properties. We utilized contact angle goniometry to probe the surface of the pNBF n films. Table 3 summarizes the advancing contact angles of water and hexadecane droplets in contact with pNBF n films. As n increases, the surfaces of the films increase in hydrophobicity and oleophobicity with the exception of pNBF10. The pNBF n films present hydrophobic and oleophobic surfaces that should have low critical surface tensions (γ_C), defined as the highest surface tension of liquid that completely wets the surface. Surfaces dominated by $-\text{CF}_3$ groups exhibit a γ_C of 6–9 mN/m, whereas $-\text{CF}_2-$ surfaces such as PTFE exhibit γ_C of ~ 18 mN/m. To estimate the critical surface tensions of the films, we used the Zisman method^{36,37} and selected a series of n -alkanes having even numbers of carbons, from hexane to tetradecane, as contacting liquids. θ_A for each of the liquids was measured on each pNBF n film, and $\cos \theta_A$ was plotted against γ_L , the surface tension of the liquid (Figure 5). A straight line fit of the data and extrapolation of the line to $\cos \theta_A = 1$ gives γ_C of the film such that a liquid with $\gamma_L \leq \gamma_C$ will completely wet the surface. pNBF8 yielded the lowest surface energy of these films with a γ_C of ~ 9 mN/m, consistent with a CF_3 -rich surface that contains some higher energy $-\text{CF}_2-$ groups. The low critical surface energy of pNBF8 and the implied dominance of $-\text{CF}_3$ groups at the surface are consistent with fluorocarbon chains orientated normal to the substrate at the liquid/polymer interface, whereas the fluorocarbon chains in the bulk of the film adopt a parallel orientation based on the large ratio of $\nu_{\text{pd}}(\text{CF}_2) : \nu_{\text{ax}}(\text{CF}_2)$ absorbances in RAIR spectra (Figure 4). Consistent with advancing contact angles of water and hexadecane, the γ_C of the pNBF n films decreased with increasing fluorocarbon side chain length with the exception of the pNBF10 films. The discontinuance of this trend for $n = 10$ may be related to its larger $\text{CF}_2 : \text{CF}_3$ ratio, exposing more $-\text{CF}_2-$ groups and reducing oleophobicity, or its presumed lower mobility to

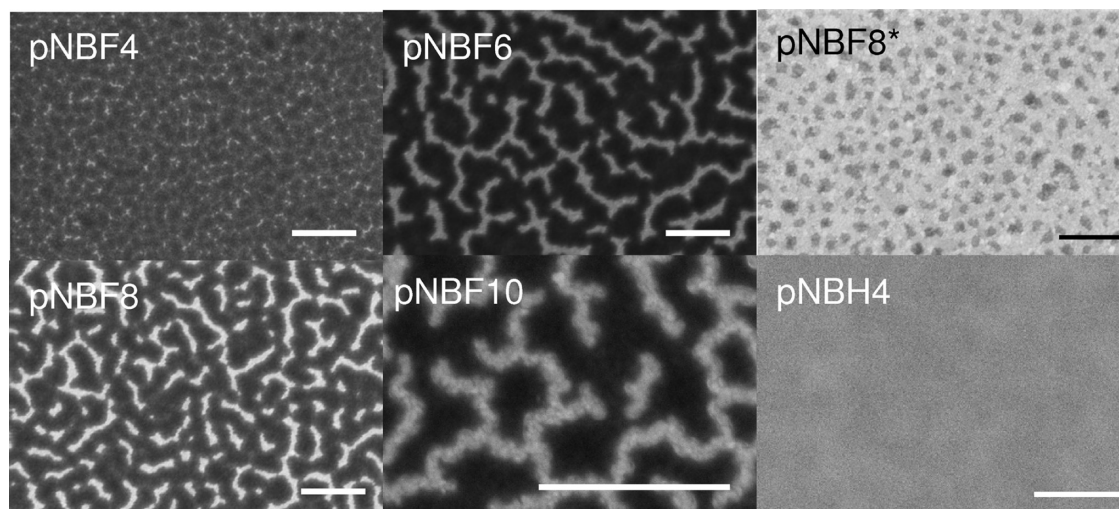


Figure 6. Scanning electron micrographs of pNBF4, pNBF6, pNBF8, pNBF10, and pNBH4 films. The pNBF6, pNBF8, and pNBF10 films were grown in 0.05 M monomer solutions for 1 min, whereas pNBF4 and pNBH4 were grown in 0.1 and 0.47 M monomer solutions for 1 min, respectively. The scale bar indicates 1 μm . *For the top right pNBF8 panel, the film has been annealed at 120 $^\circ\text{C}$ for 1 h.

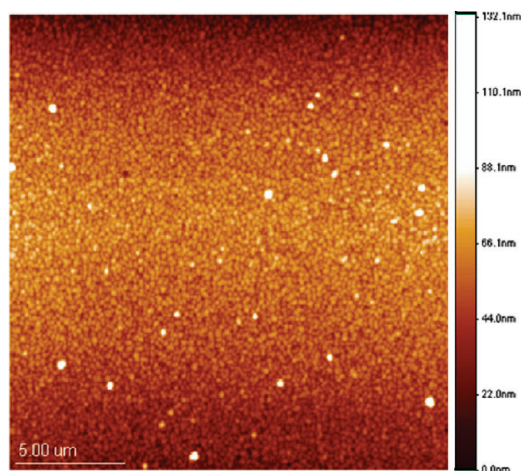


Figure 7. Atomic force microscopy tapping mode image of a pNBF10 polymer film grown by exposure to 0.05 M NBF10 in DCM for 1 min.

achieve a dense, oriented fluorocarbon film at the outer surface. The low γ_C 's of pNBF10 (~ 11 mN/m) and pNBF6 (~ 13 mN/m) indicate that the fluorocarbon chains at the surface are oriented generally normal to the substrate, but with more $-\text{CF}_2-$ groups exposed than for pNBF8. However, the fluorocarbon chains within pNBF4 do not orient at the surface like the other pNBF n films. From Figure 5, we estimate the γ_C of pNBF4 to be $\sim 19 \pm 2$ mN/m, suggesting that $-\text{CH}-$ and $-\text{CH}_2-$ groups are present at the surface as well as $-\text{CF}_2-$ and $-\text{CF}_3$ functionalities.

The Zisman plot shown in Figure 5 displays the γ_C of pNBF n films exposed to air for at least 12 h. The γ_C for freshly prepared pNBF n films were 2–3 mN/m higher than those exposed to air, which is consistent with the gradual diffusion of the fluorocarbon side chains to the air/polymer interface. The tendency for fluorocarbon moieties to partition to the air/polymer interface has been observed by others^{30,38} and is related to their mobility and the driving force to reduce interfacial free energy.

Film Morphology. We used scanning electron microscopy (SEM) in conjunction with atomic force microscopy (AFM) to investigate the morphology and topography of pNBF n films. Figure 6 displays SEM images of pNBF n films grown for 1 min using 0.1 M ($n = 4$) or 0.05 M ($n = 6, 8$, and 10) monomer concentrations in which we observed distinct light/dark patterns. As a control, we obtained SEM micrographs of pNBH4 films, also displayed in Figure 6, that do not show the patterns found in the pNBF n films. Contrast in SEM images is due to varying chemical composition of the polymer, where brighter areas correspond to higher molecular weight elements or higher electron density.³⁹ The observed patterns are not due to islands within a sparse polymer film as the AFM image in Figure 7, the barrier properties displayed in Table 2, and the critical surface energies of Figure 5 confirm the growth of dense pNBF n films. A naïve interpretation of the image might suggest that the lighter regions are fluorocarbon and the darker ones are hydrocarbon. However, the fact that pNBF n is a comblike homopolymer in which fluorocarbon and hydrocarbon regions cannot be completely separated, combined with the size (~ 50 – 100 nm) and fractional coverage of the lighter regions in Figure 6, are inconsistent with complete phase separation. Indeed, these patterns are much too large to represent the molecular structuring of a few neighboring chains, since the width of two adjacent polymer chains for pNBF10 would span ~ 2 nm. Further, the size of these lighter regions does

not scale with fluorocarbon chain length (n), and the very low critical surface energies for $n = 6, 8$, and 10 are consistent with dense fluorocarbon layers over the entire outermost surface and not just fractionally in the lighter regions.

A closer view of these regions in Figure 6, panel pNBF10, reveals the presence of small round clusters of 20–30 nm in both the lighter and darker regions. Since SEM is probing the outermost few nanometers of the surface,³⁹ the lighter regions may correspond to specific organization within polymer chains that concentrate fluorocarbon groups densely at the outer few nanometers of the surface, such as a hemispherical shell of dense fluorocarbon with hydrocarbon chains concentrated in the core. The darker regions, which still correspond to fluorocarbon groups at the outer surface, likely represent a different type of chain conformation where fluorocarbon groups are not concentrated as extensively in the outer few nanometers of the film. Annealing the film at 120 °C followed by cooling to room temperature provides sufficient energy for more chains to adopt the low-energy configuration to produce a less heterogeneous SEM image that shows a prevalence of the lighter region (Figure 6, panel pNBF8*).

Conclusions

We have utilized SI-ROMP of perfluorinated n -alkylnorbornenes to form robust partially fluorinated polymer films of tunable thicknesses ranging from tens of nanometers to micrometers on gold substrates. The length of the fluorocarbon substituent on the norbornenyl ring influences the properties of the polymer film. Increasing the length of the fluorocarbon side chain enhances the rate and extent (thickness) to which the polymer films grow from the surface. The critical surface tensions also decrease with increasing fluorocarbon chain length in which pNBF8 films yield the lowest critical surface energy, ~ 9 mN/m. Upon exposure to air, the fluorocarbon chain segments of the pNBF n films seek the air/polymer interface, enhancing the hydrophobicity and oleophobicity of the surface. SI-ROMP of pNBF n yields 20–30 nm clusters of different conformations of the polymer chains, observed as distinct light/dark patterns in SEM micrographs.

Acknowledgment. The project was supported by the U.S. Department of Energy (ER46239). R.E.F. acknowledges support from Vanderbilt University Summer Research Program. The authors thank Dr. Ed Elce (Promerus Electronic Materials) for generously providing 5-*n*-butylnorbornene monomer.

Supporting Information Available: Kinetic data for pNBF8 films, a RAIR spectrum of drop-cast pNBF10, and observational effects of solvent on pNBF n film growth. This material is available free of charge via the Internet at <http://pubs.acs.org>.

References and Notes

- (1) Wang, J. G.; Mao, G. P.; Ober, C. K.; Kramer, E. J. *Macromolecules* **1997**, *30*, 1906–1914.
- (2) Rutenberg, I. M.; Scherman, O. A.; Grubbs, R. H.; Jiang, W.; Garfunkel, E.; Bao, Z. *J. Am. Chem. Soc.* **2004**, *126*, 4062–4063.
- (3) Garbassi, F.; Morra, M.; Occhiello, E. *Polymer Surfaces: From Physics to Technology*; John Wiley & Sons: Chichester, 1998.
- (4) Tarnowski, D. J.; Bekos, E. J.; Korzeniewski, C. *Anal. Chem.* **1995**, *67*, 1546–1552.
- (5) Balachandra, A. M.; Baker, G. L.; Bruening, M. L. *J. Membr. Sci.* **2003**, *227*, 1–14.
- (6) Mocella, M. T. In *Fluorinated Compounds for Advanced IC Interconnect Applications: A Survey of Chemistries and Processes*; Elsevier Science: Amsterdam, 2003; pp 87–92.

- (7) Genzer, J.; Sivaniah, E.; Kramer, E. J.; Wang, J. G.; Xiang, M. L.; Char, K.; Ober, C. K.; Bubeck, R. A.; Fischer, D. A.; Graupe, M.; Colorado, R.; Shmakova, O. E.; Lee, T. R. *Macromolecules* **2000**, *33*, 6068–6077.
- (8) Phani, A. R.; Passacantando, M.; Santucci, S. J. *Phys. Chem. Solids* **2006**, *67*, 1703–1711.
- (9) Sivakumar, C.; Wen, T. C.; Gopalan, A.; Teng, H. *Synth. Met.* **2003**, *132*, 219–226.
- (10) Edmondson, S.; Osborne, V. L.; Huck, W. T. S. *Chem. Soc. Rev.* **2004**, *33*, 14–22.
- (11) Jennings, G. K.; Brantley, E. L. *Adv. Mater.* **2004**, *16*, 1983–1994.
- (12) Brantley, E. L.; Jennings, G. K. *Macromolecules* **2004**, *37*, 1476–1483.
- (13) Jung, D. H.; Park, I. J.; Choi, Y. K.; Lee, S. B.; Park, H. S.; Ruhe, J. *Langmuir* **2002**, *18*, 6133–6139.
- (14) Matyjaszewski, K.; Miller, P. J.; Shukla, N.; Immaraporn, B.; Gelman, A.; Luokala, B. B.; Siclovan, T. M.; Kickelbick, G.; Vallant, T.; Hoffmann, H.; Pakula, T. *Macromolecules* **1999**, *32*, 8716–8724.
- (15) Kim, J. B.; Huang, W.; Bruening, M. L.; Baker, G. L. *Macromolecules* **2002**, *35*, 5410–5416.
- (16) Wang, X. S.; Lascelles, S. F.; Jackson, R. A.; Armes, S. P. *Chem. Commun.* **1999**, 1817–1818.
- (17) Robinson, K. L.; Khan, M. A.; Banez, M. V. D.; Wang, X. S. *Macromolecules* **2001**, *34*, 3155–3158.
- (18) Brantley, E. L.; Holmes, T. C.; Jennings, G. K. *J. Phys. Chem. B* **2004**, *108*, 16077–16084.
- (19) Berron, B. J.; Graybill, E. P.; Jennings, G. K. *Langmuir* **2007**, *23*, 11651–11655.
- (20) Kim, N. Y.; Jeon, N. L.; Choi, I. S.; Takami, S.; Harada, Y.; Finnie, K. R.; Girolami, G. S.; Nuzzo, R. G.; Whitesides, G. M.; Laibinis, P. E. *Macromolecules* **2000**, *33*, 2793–2795.
- (21) Buchmeiser, M. R.; Sinner, F.; Mupa, M.; Wurst, K. *Macromolecules* **2000**, *33*, 32–39.
- (22) Liu, X. G.; Guo, S. W.; Mirkin, C. A. *Angew. Chem., Int. Ed.* **2003**, *42*, 4785–4789.
- (23) Weck, M.; Jackiw, J. J.; Rossi, R. R.; Weiss, P. S.; Grubbs, R. H. *J. Am. Chem. Soc.* **1999**, *121*, 4088–4089.
- (24) Pasquale, A. J.; Fornof, A. R.; Long, T. E. *Macromol. Chem. Phys.* **2004**, *205*, 621.
- (25) Perez, E.; Laval, J. P.; Bon, M.; Rico, I.; Lattes, A. *J. Fluorine Chem.* **1988**, *39*, 173–196.
- (26) Berron, B. J.; Payne, P. A.; Jennings, G. K. *Ind. Eng. Chem. Res.* **2008**, *47*, 7707–7714.
- (27) Harada, Y.; Girolami, G. S.; Nuzzo, R. G. *Langmuir* **2003**, *19*, 5104–5114.
- (28) Jennings, G. K.; Laibinis, P. E. *J. Am. Chem. Soc.* **1997**, *119*, 5208–5214.
- (29) Parikh, A. N.; Allara, D. L. *J. Chem. Phys.* **1992**, *96*, 927–945.
- (30) Genzer, J.; Sivaniah, E.; Kramer, E. J.; Wang, J. G.; Korner, H.; Xiang, M. L.; Char, K.; Ober, C. K.; DeKoven, B. M.; Bubeck, R. A.; Chaudhury, M. K.; Sambasivan, S.; Fischer, D. A. *Macromolecules* **2000**, *33*, 1882–1887.
- (31) Seehof, N.; Grutke, S.; Risse, W. *Macromolecules* **1993**, *26*, 695–700.
- (32) Berron, B.; Faulkner, C. J.; Fischer, R. E.; Payne, P. A.; Jennings, G. K. *Langmuir* **2009**, *25*, 12721–12728.
- (33) Hatjopoulos, J. D.; Register, R. A. *Macromolecules* **2005**, *38*, 10320–10322.
- (34) Lee, L. B. W.; Register, R. A. *Macromolecules* **2005**, *38*, 1216–1222.
- (35) Boyd, T. J.; Schrock, R. R. *Macromolecules* **1999**, *32*, 6608–6618.
- (36) Zisman, W. A. *Contact Angle, Wettability, and Adhesion*; American Chemical Society: Washington, DC, 1964; Vol. 43.
- (37) Bin Zhang, Z.; Ying, S. K.; Hu, Q. H.; Xu, X. D. *J. Appl. Polym. Sci.* **2002**, *83*, 2625–2633.
- (38) Xie, X. M.; Gengenbach, T. R.; Griesser, H. J. *J. Adhes. Sci. Technol.* **1992**, *6*, 1411–1431.
- (39) Bindell, J. B. Scanning Electron Microscopy. In *Encyclopedia of Materials Characterization*; Brundle, C. R., Evans, C. A., Wilson, S., Eds.; Butterworth-Heinemann: Boston, 1992; pp 70–84.